Non-contact boundary layer profiler using low-coherence self-referencing velocimetry

Author(s):
Kempe, Andreas; Schlamp, Stefan; Rösgen, Thomas

Publication date:
2007-08

Permanent link:
https://doi.org/10.3929/ethz-a-005707716

Originally published in:
Experiments in Fluids 43(2-3), https://doi.org/10.1007/s00348-007-0320-4

Experiments in Fluids manuscript No.
(will be inserted by the editor)

Andreas Kempe · Stefan Schlamp · Thomas Rösgen

Non–contact boundary layer profiler using low–coherence self–referencing velocimetry

Received: date / Accepted: date

Abstract A spatially self–referencing velocimetry system based on low–coherence interferometry has been developed. The measurement technique is contactless and relies on the interference between back–reflected light from an arbitrary reference surface and seeding particles in the flow. The measurement location and the flow velocity are measured relative to the reference surface's location and velocity, respectively. Scanning of the measurement location along the beam direction does not require mechanical movement of the sensor head. The reference surface (which can move or vibrate relative to the sensor head) can be either an external object or the surface of a body over which measurements are to be performed. The absolute spatial accuracy and the spatial resolution only depend on the coherence length of the light source (tens of microns for a superluminescent diode).

The prototype is an all–fiber assembly. An optical fiber of arbitrary length connects the self–contained optical and electronics setup to the sensor head. Proof–of–principle measurements in water (Taylor–Couette flow) and in air (Blasius boundary layer) are reported in this paper.

Keywords low–coherence interferometry · self–referencing velocimetry · high resolution · boundary layer profiler

1 Introduction

Velocimetry techniques for boundary layer measurements face two challenges: spatial resolution and non–intrusiveness. In most technical applications, the thickness of the boundary layers is on the order of 1 mm such that sub–millimeter resolution is required for meaningful measurements. The requirements are even higher when the viscous sub–layer and the log–layer have to be resolved [13].

Traditionally, hot–wire anemometry (or constant temperature anemometry, CTA, or constant current anemometry) has been the method of choice for such measurements (e.g., [7,8,15]). The typical diameter of the wire is on the order of micrometers. They are typically 1-2 mm long, but the spatial resolution in the wall–parallel direction is not critical. Because the measurement location is identical to the probe location, the probe has to be moved to obtain the velocity profile across the boundary layer. This makes this technique problematic for measurements over moving objects. But even over stationary surfaces, the thermal conductivity of the wall leads to systematic errors of the measured velocity [5,4].

Recently, micro–PIV has been applied to high–resolution boundary layer measurements. PIV either requires optical access from at least two directions (one for the illuminating laser sheet, the second for the camera) or a depth resolving focusing optic as in microscopy [9,10]. Depending on the geometry and the object's movement, this might not be feasible. Laser–Doppler velocimetry (LDV) lacks the required spatial resolution, which is determined by the diameter of the intersecting laser beams and the crossing angle. LDV measures the velocity component perpendicular to the long axis of the intersection ellipsoid. This means that the spatial resolution is poorest in the direction where it is most critical. With a novel technique using a tilted fringe system, the LDV intersection volume can also be resolved in the order of microns [1,2]. Distributed laser Doppler velocimetry (DLDV) [6], a reference beam LDV using low–coherence light, defines the measurement location through the focal point. The low–coherence interferometry then allows further resolution within the focal point. In this respect, the technique shares many aspects with optical coherence tomography (OCT) [14]. DLDV can be seen as a very similar technique to the approach described in this paper.

A.Kempe · Stefan Schlamp · Thomas Rösgen
Institute of Fluid Dynamics, ETH Zurich
Sonneggstrasse 3, 8092 Zurich, Switzerland
Tel.: +41-44-6325271
Fax: +41-44-6321147
E-mail: kempe@ifd.mavt.ethz.ch

In a PIV image, the flow is visible together with the object such that it should be possible to deduce the measurement location (relative to the surface) from the data without independent knowledge of the object's trajectory. Nevertheless, as mentioned, the PIV installation itself might be very challenging. CTA, LDV and DLDV on the other hand have all in common, that they are not self–referencing. At any instance, the relative location of the object to the measurement volume has to be known. If the motion is irregular or if the shape of the object changes over time, this might pose a problem in itself.

The new technique is self–referencing with respect to its vertical measurement location to an arbitrary surface and has a spatial resolution only depending on the coherence length of the light source (e.g., see interferogram Fig. 1). It measures in–plane and out–of–plane components of the velocity vector. The sensitivity to out–of–plane velocities (which are normally much lower) is tenfold (value can be adjusted) higher than for in–plane velocities. As for LDV and PIV, particle seeding is required. Conceptually, planar measurements (cf. PIV) are also possible with self–referencing capabilities.

The working principle of this new technique is explained using the example of a two–component boundary layer profiler based on the Doppler effect. The systems is spatially self–referenced relative to a surface, but applications where the sensor head is the reference follow the same principle. We want to introduce a notation for the new approach with "SR" standing for self–referencing, i.e., SR–LDV.

2 Measurement principle

The system consists of two main parts: the interferometer unit and the sensor head. Fig. 2 shows the schematic setup of the optical components in the interferometer unit of the system. A superluminescent diode (SLD, Superlum Diodes Model SLD56-HP2, 1310 nm, 10 mW) emits low–coherence light into a single–mode fiber. The dotted line in Fig. 1 is the autocorrelation function of the SLD. The coherence length is represented as the FMHW of the peak (~ 35 μm). A fiber–optical isolator protects the sensitive light source from back–reflections and guides the light to a polarization insensitive optical circulator. The circulator is used to transfer the light through a single–mode optical fiber to the sensor head, where a lens couples the light out of the fiber and onto the object surface.

A fraction of the incident light is reflected back from the surface of the test object onto the lens and back into the fiber towards the circulator, where it is deflected into the interferometer. A small fraction of the light is also reflected off the particles passing the laser beam. Fig. 3 introduces the nomenclature used subsequently. Note that the two incident beams are not used simultaneously (this would require a separate interferometer unit for each beam). Instead, it distinguishes between subsequent measurements using different incident angles relative to the flow. In Fig. 3, the reference surface is taken to be the object's surface, but this is not required.

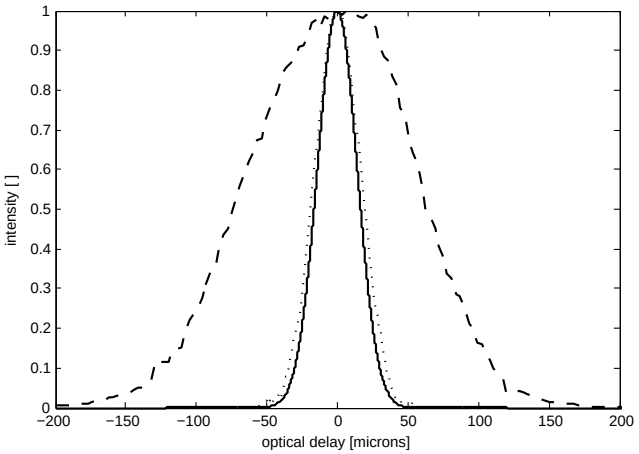

Fig. 1 Autocorrelation function of Superlum SLD-HP-56-HP: bold line = simulated data based on spectrum, dotted line = measurement with a freespace Michelson interferometer, dashed line = measurement with the all fiber assembly.

Light reflected off the test object surface is denoted as rays 1 and light scattered off the particles in the flow is denoted as rays 2. The letters distinguish between the measurements using different incident angles and the numbers refer to different reflecting objects.

All light back–reflected is fed into the two interferometer arms by a beam splitter. In the reference arm, an acousto–optical modulator (AOM, NEOS Model 26055) shifts the frequency of the light upwards by 55 MHz, corresponding to several periods within the short passage time (tens of microseconds) of the particles in the focus. The delay arm contains a motorized variable delay line (VDL, General Photonics VariDelay). The light from the two interferometer arms is recombined by another beam splitter/combiner and a broadband photoreceiver (New Focus Model 1811) serves as detector.

Only consider a single angle of incidence, measurement a, say. The path length of ray $1a$ is longer than that of ray $2a$. Denote the distance between the surface and the particle as d and the path lengths of both interferometer arms (between the two beam splitters/combiners) as l_r and l_d, respectively. If the VDL is set such that $l_r + 2d = l_d$ ("positive delay"), for example, the part of ray $1a$ going through the reference arm interferes with those parts of ray $2a$ which go through the delay arm. In a static situation the frequency of the AOM is now seen as beat signal at the detector. The same phenomena occurs if the VDL is set to $l_r - 2d = -l_d$ ("negative delay"). Then the part of ray $1a$ going through the delay arm interferes with the part of ray $2a$ which goes through the reference arm. Normally the surface reflection is orders of magnitude stronger than a particle's reflection, especially for backward scattered ligth. In case of interference

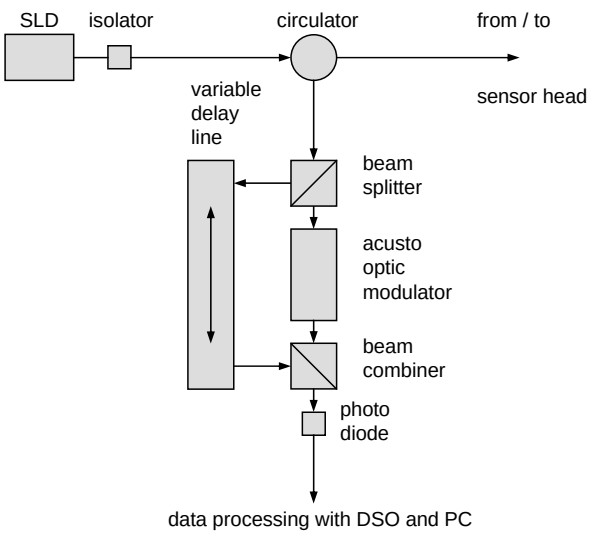

Fig. 2 Schematic setup of optical components in the interferometer unit, which also includes the light source.

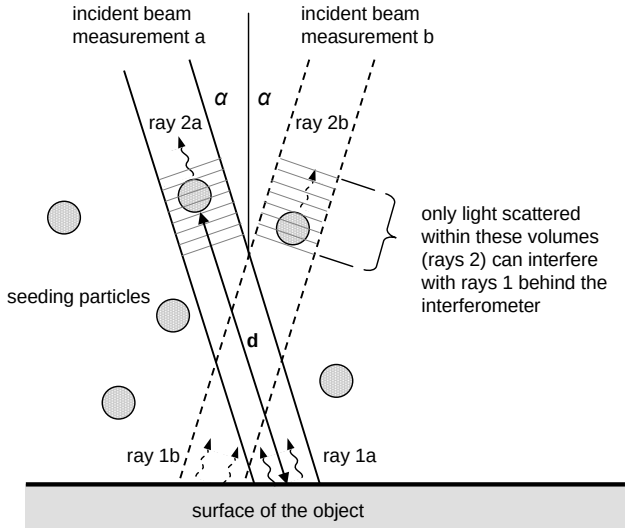

Fig. 3 Schematic setup of the interaction between laser beams and particles.

between of the two reflections, the large reference signal amplifies the weak particle reflection, thus allowing the use of an SLD with relative low optical power.

With relative movement between the particle and the surface there is a frequency difference between rays $1a$ and $2a$ due to different Doppler shifts of the two reflections. In case of interference this results in an additional frequency shift of the beat signal relative to the AOM frequency. The direction of the shift depends on the setup of the autocorrelator (positive or negative delay) and on the direction of the relative movement between the two reflections. In the absence of interference, no beat signal is present. This means that only those particles produce relevant signals, which are within a thin layer from the surface. The thickness of the layer is approximately equal to half the coherence length of the light source (typically $30 - 50$ μm for a high–power SLD). For the all–fiber assembly used for the test cases presented in this paper, there is a relatively large difference between the theoretical and the measured coherence lengths of ~ 140 μm (see dashed line in Fig. 1). This might be due to multiple reflections within the fiber optical interferometer. This broadened peak in the autocorrelation must be considered and so ~ 70 μm can be seen as the lower bound for the spatial resolution of the system.

The distance between the measurement volume and the wall can be adjusted by adjusting the delay of the VDL – independent of the vertical position of the sensor head. Irrespective of any movement of the surface, measurements are always performed at a set distance from the wall. One could say that the measurement location is in wall–fixed coordinates instead of lab–fixed coordinates as for other techniques.

Each measurement yields the relative velocity between reference surface and particle *in the direction of the laser beam*. In order to determine the wall–normal and wall–parallel velocity components separately, a second measurement with a different incidence angle is required. This is shown in Fig. 3 as beam b. These two measurement do not need to be taken simultaneously. The measurement volumes of the two beams do not necessarily coincide exactly. In fact, their offset will typically vary along the wall–normal direction. Consequently, the beams do not look at the same horizontal position. But the spacing of the beams and their diameter is small and since the resolution in wall–parallel direction is usually not crucial, this should not pose a problem.

3 Data analysis

Consider the velocity vector $\mathbf{u} = (u, v)$, where u is the wall–parallel velocity and v is the wall–normal component. Assume (without loss of generality) that the bisector of the laser beams from measurements a and b is perpendicular to the wall (as shown in Fig. 3). Interference between rays $1a$ and $2a$ produces a peak in the power spectrum at

$$f_a = \frac{2}{\lambda}(v\,cos\alpha + u\,sin\alpha) + f_{AOM} \tag{1}$$

(λ is the wavelength of the laser beams). The Doppler shift between rays $1b$ and $2b$ (from a second measurement) has the same magnitude, but opposite sign. The peak is thus at

$$f_b = \frac{2}{\lambda}(v\,cos\alpha - u\,sin\alpha) + f_{AOM}. \tag{2}$$

Denote the spacing of the two peaks as $\Delta F = |f_a - f_b|$ and the average Doppler shift as $\sum F = \frac{1}{2}(f_a + f_b) -$

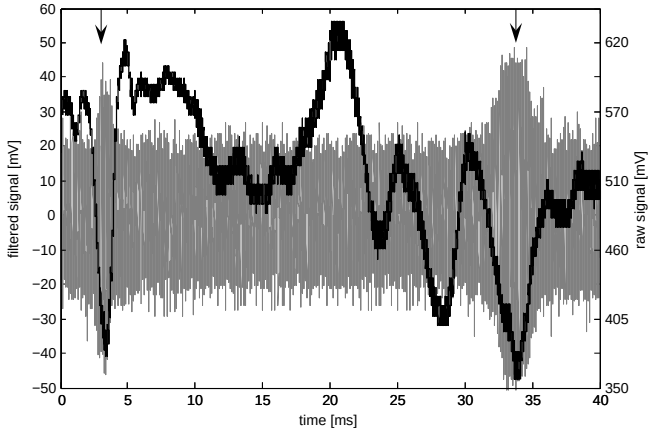

Fig. 4 Particle passages: raw signal (black) and bandpass filtered signal (gray). The arrows indicate particle passage events.[1]

f_{AOM}. The velocity vector is then obtained from

$$u = \frac{\lambda \Delta F}{4 sin\alpha} \qquad \text{and} \qquad v = \frac{\lambda \Sigma F}{2 cos\alpha}. \tag{3}$$

Since α is small, the sensitivity to wall–normal velocities ($\partial \Sigma F / \partial v$) is much larger than to in–plane velocities ($\partial \Delta F / \partial u$). The ratio of the sensitivities is $1/tan\alpha$. This is desirable, because the wall–normal velocities are much smaller than the wall–parallel velocities in boundary layer type flows.

4 Results

4.1 Signal processing

The analog signals from the photoreceiver are first filtered by a bandpass filter (Mini Circuits BBP-60) and then amplified by 36 dB with a high speed amplifier (Hamamatsu C5594-12). The preconditioned signals are then digitized with 8 bit precision by a Digital Storage Oscilloscope - DSO (LeCroy LT347L). Data is finally transferred to a PC for further analysis and storage. The sampling rate and the acquisition window length are set through the DSO. The data acquisition is triggered by a particle passing the laser beam at the correct distance from the reference surface, i.e., when the bandpass filtered signal exceeds a threshold (see also Fig. 4). The dips in the unfiltered signal during relevant particle passages (indicated by arrows) ware caused by a partial blockage of in ray 1 by the particle. The subsequent data analysis was performed by a LabView program (Ver. 7.1, National Instruments). The digitized data is first bandpass filtered with a second–order Butterworth IIR filter. The maximum of the power spectrum is extracted by an interpolating peak detection routine.

4.2 Taylor–Couette flow

The measurements between two coaxial rotating cylinders, i.e., Taylor–Couette flow, were performed to demonstrate the self–referencing capabilities. A metal cylinder (outer diameter $2r_i = 83$ mm) was placed coaxially in the center of a Plexiglas cylinder (inner diameter $2r_o = 89.3$ mm, 5 mm thick). The length of both cylinders is approx. 30 cm. They were installed vertically. The resulting gap, of about 2.85 mm, was filled with olive oil and aluminum powder (~ 50 μm diameter) as seeding. The inner cylinder could rotate with frequencies of up to $\Omega/(2\pi) = 6$ revolutions per second.

The SR–LDV sensor head was located ≈ 60 mm radially outside of the outer cylinder and slightly tilted against the flow direction. Due to the beam deflections at the curved Plexiglas surface, the angle of incidence relative to the inner cylinder is not known *a priori*. It was later calculated based on the measured frequency shifts near the wall and the known rotation rate ($\approx 15^o$). For these flow parameters the flow is laminar and the flow is parallel such that the wall–normal velocity component is known to be zero. Measurements with a single incident angle are thus sufficient.

A retro–reflecting foil was attached to the inner cylinder (the reference surface). The primary reason for this was to increase the reflection level from the reference surface *back into the collimator lens*. The reflections from the metal cylinder are otherwise very directional and thus largely miss the collection lens for sufficiently large angles of incidence. The light is not reflected from the surface of the foil, but enters it and is reflected from the internal structures. It thus covers a small path within it. This has the welcome side effect that the (optical) reference surface does not coincide with the foil surface, but lies within the foil. This allows one to measure closer to the reference surface. Normally, measurements at or near the reference surface (within the first 50 to 100 μm) require that the path lengths through both interferometer arms are nearly equal. In that case, however, all other reflections also produce interference with themselves. This results in a high background level of the beat signal, above which passing particles cannot be detected. The offset due to the path length within the reflector foil was measured to be 0.18 mm.

Owing to the spatially periodic structure of the retro–reflector, the back–reflection level is not constant, but instead highly modulated. It was also observed that, due to a shadowing effect, the reflection level from the retro–reflector and walls decreases during particle passages. However, in the bandpass filtered signal only the beat signals are visible.

In Fig. 5 the frequency–shift of the beat signal is plotted versus the optical delay of the interferometer. The surface velocity U_S of the inner rotating cylinder was

[1] Please note: The raw signal is first bandpass filtered and then amplified, thus both signal values are not directly comparable. If the raw data were digitized and then filtered, the beat signal would be less than the digitizing noise.

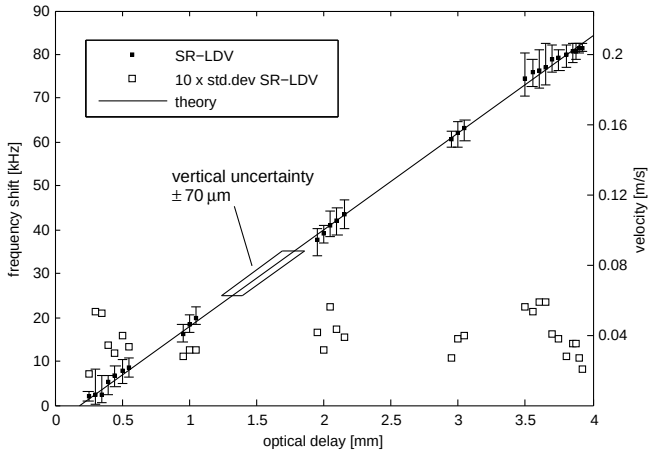

Fig. 5 SR–LDV measured Taylor–Couette flow profile, $U_S = 0.21$ m/s.

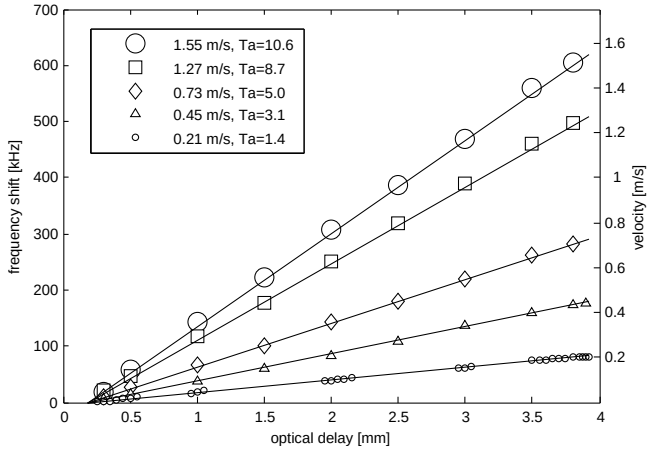

Fig. 6 SR–LDV measured Taylor–Couette flow profiles at different surface velocities. The marker size scales with standard deviation.

0.21 m/s. In a coordinate system fixed with the rotating cylinder, the fluid flow direction is negative, i.e., at the stationary outer Plexiglas wall the relative velocity is the highest and at the moving cylinder's surface it is zero, with a linear profile in–between. The error bars represent the minimum and maximum of the frequency shifts out of between 10 and 30 particle passages for each position. The standard deviation is between 1 and 2 kHz and nearly constant across the gap. Data with high spatial resolution was obtained close to each surface and within three central regions. Close to the fixed Plexiglas wall the data rate drops rapidly, because the absolute flow speed is close to zero and the number of particle passing the laser beam per unit time decreases. Note that the surface of the inner cylinder corresponds to an optical delay of 0.18 mm, the optical path within the retro–reflector.

Fig. 6 shows the frequency shift of the beat signal versus the optical delay of the interferometer at different rotation speeds of the cylinder. The data series are labelled by the surface speed of the rotating cylinder and the corresponding Taylor number

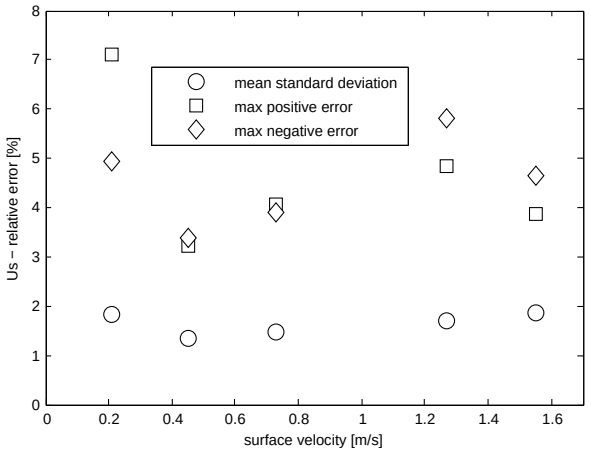

Fig. 7 SR–LDV measured Taylor–Couette flow profiles; range and uncertainty of data relative to wall speed of rotating cylinder.

$$Ta = \frac{\Omega\sqrt{r_i}\,(r_o - r_i)^{3/2}}{\mu}. \tag{4}$$

The maximum rotation speed of this test setup was approx. 6 Hz, corresponding to a surface velocity of $U_S = 1.55$ m/s. The data at all rotation speeds shows a linear behavior in accordance with theory. Fig. 7 shows the range of the measured frequency shifts and the standard deviation for each rotation speed. "Max positive error" refers to the maximum difference between the highest measured frequency shift and the mean, "max negative error" refers to the maximum difference between the lowest frequency shift and the mean. The standard deviations are averaged over the gap, because they are nearly constant for a given rotation speed. The values are plotted relative to the surface velocity. The "U_S-relative" error is $\sim 2\%$ independent of the rotation speed. The range is $\sim \pm 5\%$. Assuming that the wall–normal extent of the measurement volume is 70 μm or $\sim 0.5\%$ of the gap width, then one would expect to see variations of 0.5% of U_S in the particle speed passing the measurement volume. Thus, about one quarter of the standard deviation, can be attributed to the finite spatial resolution and the velocity gradient.

At all surface velocities, except at 1.55 m/s, the data was obtained at a sampling rate of 50 MHz and with a measurement window of 25k samples. At the highest rotational speed only $5,000$ samples have been recorded. The spectral resolution was 2 kHz and 10 kHz, respectively.

The spatially periodic structure of the retro–reflector moving with the rotating cylinder caused a temporally periodic signature in the recorded signal. Because this modulation was well outside the expected freuqnecy range

from interfering beams ($f_{AOM} \pm \Delta F$), it did could be discriminated from the useful signals. It did, however, limit the length over which a single particle passage produces a continuous interference signal. When measuring close to the stationary wall, this modulation limited the duration of the signature of a particle passage. Consequently, the acquisition window was set approximately to this value.

At higher rotations speeds the beat signal length was shorter than the acquisition window, which means that the effective real spectral resolution was lower than the theoretical value for a given frequency and the length of the acquisition window. Hence, at the highest surface speed of 1.55 m/s, a shorter acquisition window was used such that the beat signal lengths were again comparable to the acquisition window.

4.3 Blasius boundary layer

With a more powerful SLD (Exalos, EXS1320-1111, 1320 nm, 25 mW) it was also possible to perform measurements in air. For these feasibility tests the boundary layer profile of a flat plate was measured. An aluminum sharp edge, approx. 70 mm wide, 30 mm long and 1 mm thick was installed horizontally inside a small wind tunnel. As seeding particles small salt crystals with a diameter of approx. 3 μm were used. They were produced by an ultrasonic atomizer within a water–salt solution [11] and then injected in front of the wind tunnel inlet. To avoid contamination of the laboratory with the salt particles, the open loop wind tunnel discharged into a 5 m long flexible pipe guiding the exhaust air to a vent.

Optical access was provided through a clear adhesive tape. The tape was stretched across a port hole in the tunnel wall, measuring approx. 30 mm x 80 mm (see Fig. 8). The optical sensor head, a focusing lens with a diameter of about 5 mm, was installed above this window at a distance of $\approx$ 6 cm to the aluminum plate.

The focal point of the laser was set close to the surface of the flat plate, simply by focusing until the highest surface reflexion could be achieved. The aluminum surface was slightly roughened in order to obtain good reflections back into the collection lens even at higher incidence angles.

Fig. 9 shows the boundary layer profiles measured at three different flow speeds. The plotted data represents the mean value of approx. 20 particle passages for each vertical position. The reference flow rates were measured with a conventional propeller velocimeter (Schiltknecht, model number 12675). The measurement position downstream of the leading edge on the upper side of the plate was 6 mm. The incidence angle was set to $\pm 15°$ ("forward" and "backward" measurement setups). After measuring all three flow rates in the forward setup, the sensor head was rotated to the backward setup. In order to investigate the same downstream position on the flat plate, a repositioning of the sensor head was hence necessary.

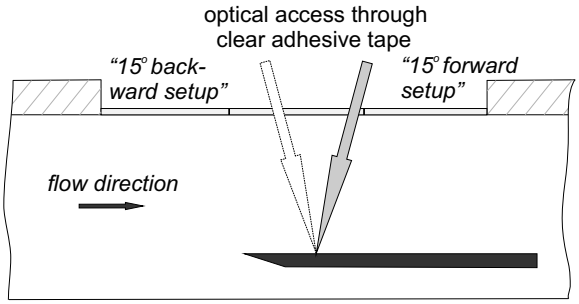

Fig. 8 Optical access to the sharp edge flat plate in the wind tunnel is provided through clear adhesive tape.

It can be seen that the measured data is in very good agreement with the blasius theory. It has to be said that the freestream velocity input (measured with the propeller meter) for the theoretical profile calculation was slightly changed (maximum by ± 0.1 m/s), in order to achieve the best fit with the measured profile. Nevertheless, for the wall–parallel velocity component, only a few points show a small deviation to the theoretical boundary layer shape ($\pm 1\%$). Agreement for the out–of–plane velocity (scaled up in the plot by a factor of 10) is worse, but still satisfactory. Note that the measurement uncertainty (in absolute terms) is independent of the flow velocity. This leads to large relative errors for low flow velocities.

In contrast to the measurements in liquid, no retro–reflecting foil was used to generate the reference reflection. Hence, the zero delay setting of the interferometer is equal to the zero wall normal position. As mentioned before, for measurements very close to the surface this leads to large beat signal due to interference of each signal with itself. Therefore, measurements within the first 150 μm above the surface could not be obtained. Since this value only depends on the light source, but is independent of the flow, the spatial resolution in terms of wall

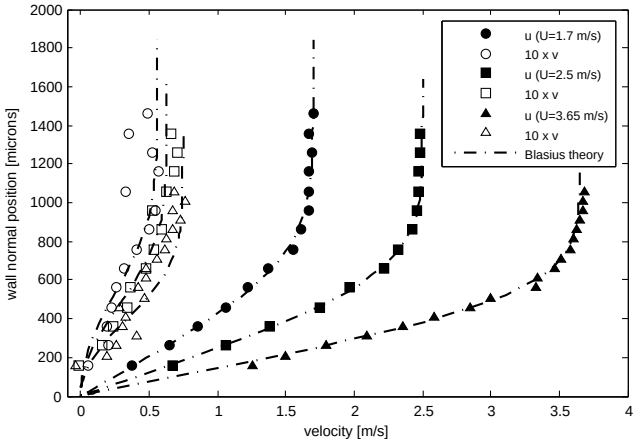

Fig. 9 Measured and theoretical Blasius profiles. (U = 1.7, 2.5, 3.65 m/s, Re_x = 680, 1000, 1400)

units will depend on the flow. For the intermediate flow speed of $U = 2.5$ m/s ($Re_x = 1000$), this corresponds to $y^+ \approx 3.5$. If desired, it would also be possible to use a retro–reflector in gaseous flows, allowing measurements much closer to the wall.

5 Measurement uncertainty considerations

5.1 General measurement precision

Even though various error sources for laser–Doppler velocimetry are discussed in the literature (e.g. see Ref. [3] and references given therein), the overall measurement error for a specific system and for a specific application is not easy to estimate. In addition, to validate a new LDV sensor concept a simple theoretical model might not be feasible. Alternatively, validations are done experimentally by measuring a well–known phenomenon and comparing the results with the theory.

For this novel boundary layer profiler this was done with a number of generic flows, i.e., a Poiseuille flow, a Taylor–Couette flow and a laminar Blasius boundary layer. The estimation of the errors in these specific experiments was done under the assumption of a theoretical perfect flow (no turbulence). To make the results comparable, the optical arrangement of the sensor head was not modified (lens diameter 5 mm, measurement distance approx. 60 mm, observation angle ±15°).

In general, a simple lower limit for the frequency measurement accuracy can be given by

$$\Delta f_{min} \sim \frac{1}{\Delta t}, \tag{5}$$

where Δt is the length of the observed particle burst. This could be improved by a factor of about 2 due to the interpolation scheme for the peak detection in the power spectrum. However, this value strongly depends on the experimental setup and cannot be taken as constant. In the following only two sources of error are described, which are significant for the self-referencing setup.

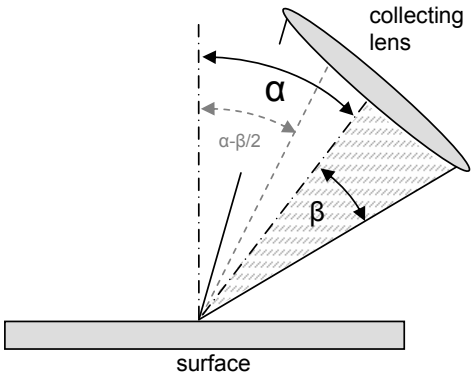

Fig. 10 Aperture broadening through finite collection angle 2β and shadowing effect through partial blockage of the aperture by passing particles.

5.2 Aperture broadening

As shown in Fig. 10, the angle of scattered light can vary from $\alpha - \beta$ to $\alpha + \beta$ depending on the aperture of the collecting lens. Since the Doppler shift of the backscattered light among others also depends on the observation angle, this results in a broadening of the received Doppler frequency signal. In a first estimate (see [12] for experimental validation) the limits of this effect can be determined as

$$\Delta f_{broad} = \pm \frac{2u}{\lambda}\, sin\beta. \tag{6}$$

The mean Doppler shift for a reference beam LDV depends on the incidence angle α

$$\Delta f_{main} = \frac{2u}{\lambda} sin\alpha. \tag{7}$$

The ratio of the broadening effect and the mean Doppler shift is then

$$\zeta_{broad} = \pm \frac{sin\beta}{sin\alpha}. \tag{8}$$

Taking the mean Doppler shift as the quantity of interest for flow velocity measurements, this ratio can be seen as the maximum impact factor of aperture broadening onto the measurement value.

5.3 Shadowing effect

The shadowing effect is specific to self–referencing LDV. Since the reflection from the particle and reference surface are in line outside of the interferometer, a particle crossing the laser beam can partially hide the reflections of the surface during its passage (see Fig.4). To make a self–referenced measurement, the light from the particle and from the surface has to interfere to generate a signal. In case of interference, a relatively large signal from the surface can act as an amplifier for the particle reflection. Therefore, one has to make sure that while a particle passes the focus, sufficient surface reflections are also visible.

There are also consequences for the measured velocity. Consider a particle passing through the shaded region in Fig. 10. The particle will reflect light symmetrically back onto the lens. The broadening will then be as given in Eq. 6. At the same time, the particle blocks parts of the lens for light reflected by the surface. The effective collection angle is thus less than 2β and the mean angle is not α, but $\alpha - \beta/2$ (neglecting that the lens is spherical and assuming that one half of the lens is blocked completely).

In case of a moving surface this leads to a shifted beat signal and in turn to a false measurement of the velocity difference between surface and particle. In contrast to the aperture broadening, this effect cannot be compensated by an interpolation mechanism for the frequency

determination. The absolute frequency error scales with β, but the relative error scales like that for the broadening effect (Eq. 8).

6 Conclusions

An optical velocimetry technique was presented which is based on low–coherence interferometry. The extent and the error of the location of the measurement volume is comparable to the coherence length of the light source (tens of micrometers). The measurement location is set relative to a reference surface (which could be the surface of a moving object). The measurement location can be scanned along a line without mechanical movement of the sensor head. As for standrad LDV techniques particle seeding is necessary. Multiple components of the velocity vector can be measured using a single interferometer and light source. This can be achieved by either taking measurements subsequently from different directions or by a multi–beam setup. A multi–beam setup can take advantage of the fact that the same light source can be used for all velocity components, but that a separate interferometer is required for each observation direction. This, in turn, requires a separate collection lens for each direction and thus a separate fiber.

The data rate depends on the number of particles crossing the sample volume per unit time. It is thus proportional to the seeding density, but also to the flow velocity and inversely proportional to the extent of the sample volume in each direction. There hence exists a trade–off between spatial resolution and data rate. In the measurements presented in Sec. 4, the data rate was only one particle passage every few seconds. Even at higher seeding densities or flow velocities, turbulent time scales can clearly not be resolved. Yet, histograms for the velocitiy can be accumulated over time.

The measurement range depends on the power of the light source, the reflection levels of the reference surface and the particles (i.e., particle size), and the collection angle of the optics (i.e., lens diameter and distance to the measurement volume). In the first test series a lens with a diameter of 5 mm, a measurement distance of 60 mm (collection angle of approx. 5°), aluminum powder as particle seeding (approx. 50 μm diameter) and a 10 mW light source were used. This allowed a measurement range of approx. 4 mm, without moving the sensor head. Improvements could be made using a more powerful light source. For measurements in liquids the measurement range was increased by a factor of 2. Hence, the focal point does not need to be exactly at the surface, which facilitates the handling of the sensor. With the increase in light power, measurements in air could also be demonstrated. With a collection angle of approx. 5° and small salt crystals as seeding (1-4 μm diameter) a measurement range of approx. 2 mm without relocating the sensor head was possible.

Decreasing the collection angle leads to an elongated focal point, which in turn increases the range in which the sensor front end does not need to be moved to collect particle reflections, as well as the absolute measurement range in respect to the surface (i.e., the region where enough surface reflections are available). It also increases the accuracy of the velocity measurement, due to longer passage times. On the other hand it significantly reduces the reflection level from the particles. Due to the autocorrelator setup of the interferometer and the large zero delay signal, measurements within the first 150 μm above the wall could not be performed directly, but using a retro–reflecting foil.

Further developments focus on the handling of the sensor. Although the sensor has self–referencing capabilities, measurements are only possible when the focus is set close to the surface, especially when using small particles as in air flows. To overcome this limitation an auto–focusing optic will be implemented. Furthermore, with the actual SR–LDV single beam setup the incident angle to the surface must be known, which is a direct source of uncertainty. With a different SR–LDV dual–beam configuration, currently under investigation, the angle of incidence will be inherently known. This setup also adds a genaral interferometer offset, which makes the retro–reflector obsolte and which directly allows for 1d2c measurements (without rotating the sensor head as in single beam SR–LDV). Additional provisions are made to adapt the system to 2d2c measurments by the use of a planar surface scanning technique.

References

1. Büttner, L., Czarske, J.: A multimode–fiber laser–Doppler anemometer for highly spatially resolved velocity measurements using low–coherence light. Measurements Science and Technology **12**, 1891–1903 (2001)
2. Büttner, L., Czarske, L.: Spatial resolving laser Doppler velocity profile sensor using slightly tilted fringe systems and phase evaluation. Measurement Science and Technology **14**, 2111–2120 (2003)
3. Durst, F., Melling, A., Whitelaw, J. H.: Theorie und Praxis der Laser–Doppler–Anemometrie. Braun, Karlsruhe (1987)
4. Durst, F., Zanoun, E. S.: Experimental investigation of near–wall effects on hot–wire measurements. Experiments in Fluids **33**(1), 210–218 (2002)
5. Durst, F., Zanoun, E. S., Pashtrapanska, M.: In situ calibration of hot wires close to highly heat–conducting walls. Experiments in Fluids **31**(1), 103–110 (2001)
6. Gusmeroli, V., Martinelli, M.: Distributed laser Doppler velocimeter. Optics Letters **16**(17), 1358–1360 (1991)
7. Häggmark, C. P., Bakchinov, A. A., Alfredsson, P. H.: Measurements with a flow direction boundary–layer probe in a two–dimensional laminar separation bubble. Exp. Fluids **28**, 236–242 (2000)
8. Ligrani, P. M., Bradshaw, P. H.: Spatial resolution and measurement of turbulence in the viscous sublayer using subminiature hot–wire probes. Exp. Fluids **5**, 407–417 (1987)
9. Lin, H. J., Perlin, M.: Improved methods for thin, surface boundary layer investigations. Exp. Fluids **25**, 431–444 (1998)

10. Meinhart, C. D., Wereley, S. T., Gray, M. H. B.: Volume illumination for two–dimensional particle image velocimetry. Measurements Science and Technology **11**, 809–814 (2000)
11. Rusch, D., Kempe, A., Rösgen, T.: Seeding of high temperature air flow (2006). Experiments in Fluids, submitted 04-06
12. Saarimaa, R.: A laser Doppler velocimeter for surface velocity measurement. Journal of Physics E **12**, 600–603 (1979)
13. Schlichting, H., Gersten, K.: Boundary–Layer Theory. Springer Verlag Berlin (2000)
14. Tomlins, P. H., Wank, R. K.: Theory, developments and applications of optical coherence tomography. Journal of Physics D **38**(15), 2519–2535 (2005)
15. Wolff, S., Brunner, S., Fottner, L.: The use of hot–wire anemometry to investigate unsteady wake–induced boundary–layer development on a high-lift lp turbine cascade. Journal of Turbomachinary **122**, 644–650 (2000)